

Beyond directions: Rotation sets for triaxial diffusion encoding by geometric filter optimization (GFO)

Sune Nørhøj Jespersen^{1, 2, *} and Filip Szczepankiewicz³

¹*Department of Clinical Medicine, Aarhus University, Denmark*

²*Department of Physics and Astronomy, Aarhus University, Denmark[†]*

³*Department of Medical Radiation Physics, Lund University, Sweden*

Abstract

I. PURPOSE

We aim to improve the accuracy of the diffusion-weighted powder average signal for diffusion encoding with arbitrary shape. This enables a categorical improvement in all quantification based on, for example, tensor-valued diffusion encoding at no additional cost to acquisition time.

II. METHODS

We propose a method to generate optimal rotation sets that are applied to the diffusion encoding gradient waveform to yield powder averages with maximal accuracy. The method, termed “Geometric Filter Optimization” (GFO), amounts to designing an appropriate sampling filter which is approximately flat in the relevant part of the associated frequency space. We characterize the filter properties and benchmark the performance in terms of the accuracy and precision of powder averages and higher order rotational invariants.

III. RESULTS

GFO filters were found to have much smaller spectral leakage than other designs. We found that GFO leads to marked improvements in precision and accuracy in powder averaging over generic diffusion encoding objects, and similarly in higher order rotational invariants, although for sufficiently high b and N , accuracy, but not precision, deteriorated compared to electrostatic repulsion.

IV. CONCLUSION

GFO provides an efficient recipe for obtaining orientations for powder averaging of signals with non-axisymmetric diffusion encoding. It places no additional demands on gradient system performance and can be used to shorten scan time.

* sune@cfin.au.dk

† Present address: CFIN, Universitetsbyen 3, Building 1710, 8000 Aarhus, Denmark.

¹ **Abbreviations:** DDE, Double Diffusion Encoding; LTE, Linear b-Tensor Encoding, STE, Spherical b-

V. INTRODUCTION

The encoding in diffusion MRI (dMRI) is most commonly performed along a single direction per shot; the field gradient on each axis is applied in a synchronous manner to sensitize the signal to motion along that direction [1]. Although this conventional approach has had tremendous success, it is unable to probe certain features of tissue microstructure, which has motivated the development of alternatives.

Tensor-valued diffusion encoding, sometimes referred to as multidimensional dMRI, employs multiple pulsed field gradients (multiple diffusion encoding [2, 3]) or continuously modulated asynchronous gradient waveforms, to encode diffusion along more than one direction per shot [4]. Unlike conventional diffusion encoding, this encoding can no longer be described by a single vector but rather requires a second-order tensor that can have a rank of up to three. This means that the diffusion encoding, in addition to its strength and direction, has a "shape" [5, 6]. Indeed, it is the combination of multiple b-tensors of different shapes that enables the measurement of microscopic fractional anisotropy [7, 8] and the disentanglement of isotropic from anisotropic diffusional kurtosis [9]. Acquiring data with multiple b-shapes has also been shown to remove the degeneracy in the Standard Model parameter estimation [10–13].

Several methods in dMRI are based on the analysis of the so-called signal powder average [7, 8, 14–17]. Briefly, the powder-average is the directional average of the signal on a given b-shell, intended to approximate the signal in a substrate in which the orientations of all domains are isotropically distributed, like in a powder [18]. In turn, this enables a compact mathematical representation of the signal which is generally easier to use in estimation [19, 20]. When using encoding objects that are axi-symmetric, e.g., conventional diffusion encoding or tensor-valued encoding with only one or two unique eigenvalues, the set of rotations that yield an accurate powder average is straightforward to produce using, for example, electrostatic repulsion of point charges on the mantle of a sphere [14, 21]. By contrast, for triaxial encoding—b-tensors with three distinct eigenvalues without a symmetry axis—an isotropic distribution of encoding orientations requires additional considerations [8, 22–24].

The aim of this work is to propose a novel technique for generating optimal sets of

Tensor Encoding, SM, Standard Model; SMEX, Standard Model with EXchange; fODF, fiber Orientation Distribution Function; elstat, electrostatic repulsion; GFO, geometric filter optimization

rotations that yield accurate powder-averages and precise higher order rotational invariants for triaxial encoding objects.

VI. THEORY

We begin by briefly listing some basic but necessary properties of harmonic analysis on the rotation group $\text{SO}(3)$, and note the factorization of kernel and fiber orientation distribution functions (fODF) in the Standard Model extended to tensor-valued diffusion encoding and triaxial diffusion tensors in the Appendix.

In this work, we use h and g to denote both the abstract elements of $\text{SO}(3)$ and, by a slight abuse of notation, their corresponding 3×3 rotation matrices in the defining representation. Integrals over $\text{SO}(3)$ are normalized such that

$$\int_{\text{SO}(3)} dg = 1.$$

For example, we can take $dg = \sin \beta d\alpha d\beta d\gamma / (8\pi^2)$ and α, β, γ are ZYZ active rotation Euler-angles $R(\alpha, \beta, \gamma) = R_z(\alpha)R_y(\beta)R_z(\gamma)$.

For functions $f(g)$ from $\text{SO}(3)$ to \mathbb{C} , we define the Fourier Transform

$$\begin{aligned} f(g) &= \sum_{l=0}^{\infty} \sum_{m,n=-l}^l (2l+1) \mathcal{D}_{mn}^{l*}(g) f_{mn}^l \\ &= \sum_l (2l+1) \text{Tr} \left(f^l \mathcal{D}^l(g^{-1}) \right) \\ &\Updownarrow \\ f_{mn}^l &= \int_{\text{SO}(3)} \mathcal{D}_{mn}^l(g) f(g) dg, \end{aligned}$$

where $\mathcal{D}^l(g)$ are the Wigner matrices, constituting irreducible representations of $\text{SO}(3)$, and thereby a complete set by the Peter-Weyl theorem. Note that f^l and \mathcal{D}^l are both complex matrices of size $(2l+1)$ -by- $(2l+1)$. As usual, convolution factorizes for Fourier transforms

$$\begin{aligned} F(g) &\equiv (f_1 \otimes f_2)(g) \equiv \int_{\text{SO}(3)} f_1(gh^{-1}) f_2(h) dh \\ &\Updownarrow \\ F^l &= f_1^l f_2^l. \end{aligned}$$

For concreteness, we will exemplify the diffusion-weighted signal assuming anisotropic Gaussian diffusion

$$S(\mathbf{B}) = \exp(-B_{ij}D_{ij}) = \exp(-\mathbf{B} : \mathbf{D}), \quad (1)$$

where D is the diffusion tensor and B is the diffusion weighting tensor (b-tensor), defined in terms of the effective diffusion encoding gradient waveform $\mathbf{G}(t)$ as

$$B_{ij} = \gamma^2 \int_0^T dt \int_0^t dt_1 \int_0^t dt_2 G_i(t_1) G_j(t_2), \quad (2)$$

with a b-value defined by its trace, $b = \sum_i B_{ii}$. However, we note that the theory described herein generalizes to any other diffusion signal model or representation with any functional dependence on the gradients through B , e.g., multi-Gaussian diffusion.

For linear b-tensor encoding (LTE) with $B = b\hat{\mathbf{g}}\hat{\mathbf{g}}^T$, the powder average (\bar{S}) of the diffusion-weighted signal (S) is

$$\bar{S}(b) \equiv \int_{S_2} S(b, \hat{\mathbf{g}}) d\hat{\mathbf{g}}, \quad \text{with } \int_{S_2} d\hat{\mathbf{g}} = 1. \quad (3)$$

In practice, the integral is approximated by a weighted average of signals acquired along some carefully chosen directions, e.g., using the principle of electrostatic repulsion[14, 21], $\bar{S} \approx \sum_i w_i S(\hat{\mathbf{g}}_i)$ with weights $\sum_i w_i = 1$. The natural generalization to arbitrary b-tensor encoding involves an average over all orientations of B , i.e., an average over the rotation group $SO(3)$ [8, 23]. For that, we define \mathbb{B} as the trace-normalized b-tensor in its principal axis system, i.e.,

$$\mathbb{B} = \frac{1}{b} \begin{bmatrix} b_1 & 0 & 0 \\ 0 & b_2 & 0 \\ 0 & 0 & b_3 \end{bmatrix}. \quad (4)$$

where the b -value $b = b_1 + b_2 + b_3$. The full landscape of b-tensor shapes is illustrated in Fig. 1, and we will focus on triaxial b-tensors with $b_1 > b_2 > b_3 \geq 0$. We then consider the signal as a function of a rotation, $g \in SO(3)$:

$$g \mapsto S(g) \equiv S(b, g\mathbb{B}g^{-1}) \in \mathbb{C}$$

with the dependence on b and \mathbb{B} being implicit. For any \mathbb{B} , the true signal powder average is

$$\bar{S}(b, \mathbb{B}) \equiv \int_{SO(3)} S(g) dg \quad (5)$$

The practical version, which involves a weighted signal average, can be expressed using a filter $f(h) = \sum_i w_i \delta(h - h_i)$

$$\bar{S} \approx \hat{S}(g) \equiv \sum_{i=1}^N w_i S(gh_i^{-1}) = \int_{SO(3)} S(gh^{-1}) f(h) dh, \quad (6)$$

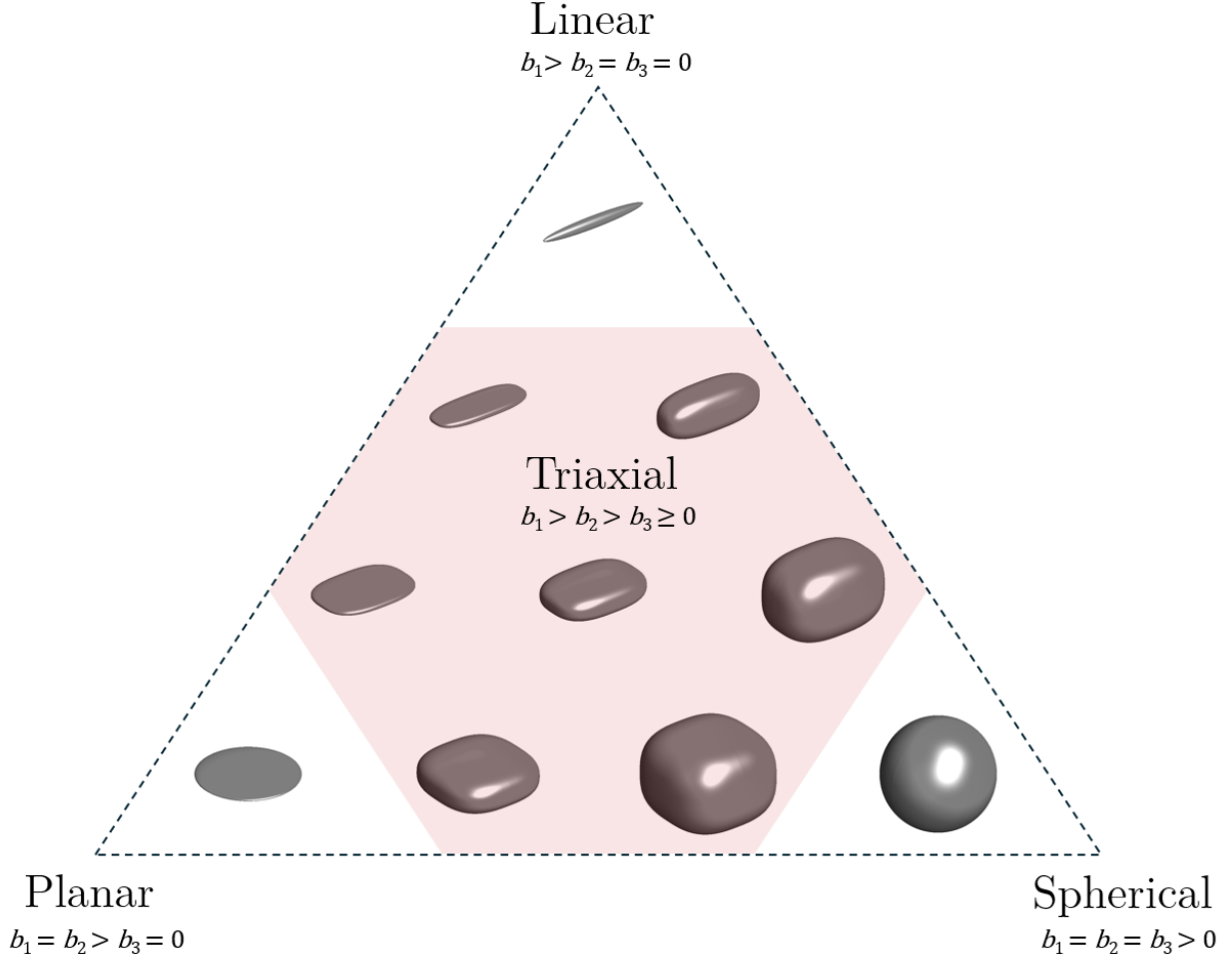


FIG. 1: The landscape of b-tensors includes all possible combinations of eigenvalues and can be visualized as glyphs in a triangle wherein the corners are the only axi-symmetric cases: linear, planar, and spherical. The interior of this triangle (pink area) indicates all other b-tensor shapes, each with three unique eigenvalues, i.e., the b-tensors are triaxial.

and, hence, $\widehat{S}^l = S^l f^l$. Thus, the filter is defined in terms of its weights w_i and sampling points h_i . Comparing Eqs. 5 and 6 we see that perfect powder averaging is achieved by $f = 1$. Hence, a good filter is characterized by $f \approx 1$. In terms of its SO(3) Fourier-coefficients, this implies that $f_{mn}^l \approx \delta_{l0}\delta_{m0}\delta_{n0}$. From the filter definition, $f_{mn}^l = \sum_i w_i \mathcal{D}_{mn}^l(h_i)$, or expressed in matrix form as $\mathbf{f} = \mathbf{Aw}$, where \mathbf{A} contains the Wigner-D matrices $\mathcal{D}_{mn}^l(h_i)$ with lmn along rows (up to some L), i along columns, and \mathbf{f} stacks the target coefficients f_{mn}^l . In terms of dimensions, \mathbf{w} is $N \times 1$, \mathbf{A} is $N_L \times N$ and \mathbf{f} is $N_L \times 1$, where $N_L = \sum_{l=0}^L (2l+1)^2 = 1/3(1+L)(1+2L)(3+2L)$. We thus seek to minimize

$$\|\mathbf{VAw} - \mathbf{Vf}\|^2 \quad (7)$$

with V an $N_L \times N_L$ diagonal matrix of user-defined weights across l . An equivalent formulation for S^2 (LTE) was used in [25–27], to optimize weights given directions based on electrostatic repulsion. This scheme can be extended to $\text{SO}(3)$ [23].

Here, we propose "Geometric Filter Optimization" (GFO) where we fix the weights at $w_i = 1/N$ and instead optimize the rotations h_i such that $f \approx 1$. Then the cost function reduces to

$$\begin{aligned}
J(\{h_i\}_{i=1\dots N}) &= (\mathbf{Aw} - \mathbf{f})^\dagger V^\dagger V (\mathbf{Aw} - \mathbf{f}) \\
&= k + \frac{1}{N^2} \sum_{j,k=1}^N \sum_{l=0}^L V_{ll}^2 \sum_{m,n=-l}^l \mathcal{D}_{mn}^l(h_j) \mathcal{D}_{mn}^l(h_k)^* \\
&= k + \frac{1}{N^2} \sum_l V_{ll}^2 \sum_{jk} \chi^l(h_j h_k^{-1}) \\
&= k + \frac{1}{N^2} \sum_l V_{ll}^2 \sum_{jk} \frac{\sin[(2l+1)\beta_{jk}/2]}{\sin(\beta_{jk}/2)}, \quad (8)
\end{aligned}$$

where k is a constant, $\chi^l(h) = \text{Tr}(\mathcal{D}^l)$ are the $\text{SO}(3)$ group characters, and β_{jk} is the rotation angle of $h_j h_k^{-1}$. In the quaternion representation, $h \leftrightarrow q$, this simplifies to $\chi^l(h_j h_k^{-1}) = U_{2l}(q_j \cdot q_k)$, where U_{2l} is a Chebyshev polynomial of the second kind.

To guide the selection of V , we consider the variance of the estimated signal power average, $\text{Var}[\hat{S}]$, which can be shown to be exactly

$$\text{Var}[\hat{S}] = \sum_{l>0} (2l+1) \sum_{m,k} \left| \sum_n S_{kn}^l f_{mn}^{l*} \right|^2. \quad (9)$$

Defining the rotational invariants S_l (and band powers E_l), in analogy to linear b-tensor encoding in the Standard Model [16], we get (see also Appendix)

$$E_l(S) \equiv \sum_{m,n} |S_{mn}^l|^2 = (2l+1)S_l^2, \quad (10)$$

$$E_l(f) \equiv \sum_{m,n} |f_{mn}^l|^2 = (2l+1)f_l^2, \quad (11)$$

and applying Cauchy–Schwarz inequality to the inner sum in (9), we arrive at

$$\text{Var}[\hat{S}] \leq \sum_{l>0} (2l+1) E_l(S) E_l(f). \quad (12)$$

This upper bound shows that the contribution of band l is governed by the product of the band powers of S and of the sampling filter f . On the other hand, up to a constant, our GFO cost is $\sum_l V_{ll}^2 f_l^2$. Identifying these structures suggests choosing

$$V_{ll}^2 \propto (2l+1)E_l(S),$$

with $E_l(S)$ estimated from a representative ensemble of signals. With this choice, minimizing the GFO cost directly targets the bands that have the largest contribution to the variance of the estimated powder average.

A rough generic estimate of the variance in terms of signal power alone can be made by assuming that the orientations are uniform. Then, for $l > 0$, $\langle \mathcal{D}_{mn}^l(h_j) \mathcal{D}_{mn}^l(h_k)^* \rangle = \delta_{jk}/(2l+1)$, and therefore $\langle f_l^2 \rangle = (2l+1)/N$. Hence, we can approximate an upper bound for the variance of powder averages, according to

$$\text{Var}[\hat{S}] \lesssim \frac{1}{N} \sum_{l>0} (2l+1)^3 E_l(S). \quad (13)$$

So far, we have not exploited any properties of the class of signals we are considering. However, symmetry properties restrict the Fourier components of the signal, and therefore we can focus our efforts on controlling only the relevant filter components. Diffusion signals that depend only on g via $B = g\mathbb{B}g^{-1}$ are invariant to transformations $g \rightarrow gK$ for $K \in \{I, R_x(\pi), R_y(\pi), R_z(\pi)\}$, the dihedral group $D_2 \subset \text{SO}(3)$, since

$$(gK)\mathbb{B}(gK)^{-1} = g(K\mathbb{B}K^{-1})g^{-1} = g\mathbb{B}g^{-1},$$

as $K\mathbb{B}K^{-1}$ just inverts two eigenvectors. In short, $S(g)$ is right-invariant to D_2 . It follows that $S^l = S^l \mathcal{D}^l(K)$ for all $K \in D_2$, and that S^l therefore lies in the image of the projector

$$P^l = \frac{1}{4} \sum_{K \in D_2} \mathcal{D}^l(K), \quad (P^l)^2 = P^l$$

which means that $S^l = S^l P^l$. This can be shown to imply, among other things, that the entire $l = 1$ sector as well as all S_{mn}^l with odd n vanish. By contrast, and unlike for LTE, the odd- l coefficients do not vanish in general; however, they are relatively small because the projector P^l has a lower-dimensional image. Since the true signal is right-invariant under the action of D_2 , i.e., $S(gK) = S(g)$ for all $K \in D_2$, it is natural to require the estimated powder average to respect the same invariance. This is achieved by symmetrizing the sampling filter over the right action of D_2 , defining

$$f_{D_2}(h) \equiv \frac{1}{4} \sum_{K \in D_2} f(hK).$$

The corresponding estimate,

$$\hat{S}(g) = \int_{\text{SO}(3)} S(gh^{-1}) f_{D_2}(h) dh,$$

is then right-invariant by construction. In Fourier space, this symmetrization amounts to projecting the filter coefficients onto the image of the projector so that $f_{D_2}^l = f^l P^l$. Consequently, only the projected components $f^l P^l$ contribute to the estimate. In terms of $\text{SO}(3)$, this means we optimize the point wise average of J over D_2

$$\frac{1}{4^N} \sum_{K_1 \dots K_N \in D_2} J(h_1 K_1, h_2 K_2, \dots, h_N K_N) = \\ k + \frac{1}{4N^2} \sum_{K \in D_2} \sum_l V_{ll}^2 \sum_{jk} \chi^l(h_j K h_k^{-1}). \quad (14)$$

We refer to this variant, which requires four times as many computations, as "GFO + D_2 ". Note that this cost function is a function on the right-coset, gD_2 .

The principle of electrostatic repulsion on $\text{SO}(3)$ [23] can also be extended to take into account D_2 symmetry. To do so, we replace the geodesic distance $d(h_i, h_j)$ between two rotations h_i and h_j , by its minimum over their right-cosets, $h_i D_2$ and $h_j D_2$, i.e., $\min(d(h_i K_1, h_j K_2))$, where the minimum is taken over $K_1, K_2 \in D_2$. These two optimization principles will be abbreviated "elstat" and "elstat + D_2 ".

VII. METHODS

We perform minimization of Eqs. (8) and (14) over rotations parameterized in terms of quaternions. A global optimization algorithm "particleswarm" (Matlab, version *R2025b*. The MathWorks, Inc., Natick, Massachusetts, United States) was used. We quantified the performance of the powder averages in terms of the coefficient of variation (CV) of powder-averaged signals; the ideal powder average is stationary under rotations of the object meaning that a lower CV is better. Assuming a signal from Gaussian diffusion (Eq. (1)) we calculated CV across 1183 rotations (from an $L = 6$ Euler grid, see below) of the diffusion tensor, $D = \text{diag}(0.1, 0.1, 2.8) \text{ } \mu\text{m}^2/\text{ms}$, for sets of 4 to 64 rotations of the b-tensor $\mathbb{B} = \text{diag}(0, 1/3, 2/3) \text{ ms}/\mu\text{m}^2$. Seven schemes for generating the rotation sets were compared: (i) Haar-random rotations; (ii) quasi-uniform grid; (iii) electrostatic repulsion (elstat) and (iv) its D_2 variant; (v) GFO and (vi) its D_2 variant; and finally, (vii) a "naive scheme". The quasi-uniform grid was constructed on the basis of Hopf fibration coordinates in $\text{SO}(3)$ as described in [28]. The naive scheme was constructed by first selecting rotation axes using the principle of electrostatic repulsion on the 2-sphere[21], followed by selecting rotation angles φ uniformly in $(\varphi - \sin(\varphi))/\pi$ and randomly paired with axes. This ensures Haar-uniformity on $\text{SO}(3)$.

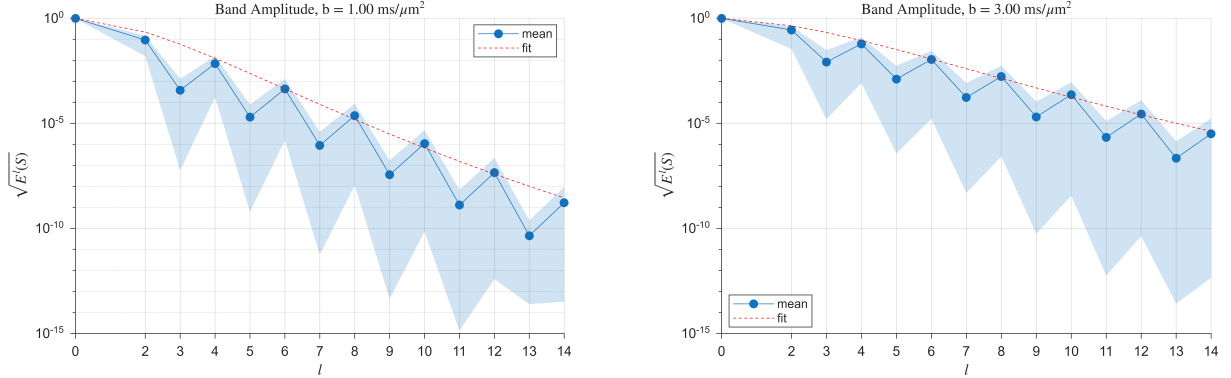


FIG. 2: Relative band amplitudes as a function of l -band for 100 random diffusion tensors show that the power is dominated by even- l bands and that power dissipates rapidly with l . The blue shaded region indicates the range over the distribution and circles show the mean. The red dashed line shows the Sobolev form $(1 + (l(l + 1))/\kappa^2)^{-s}$ fit to the data for even l , giving $\kappa \simeq 6.3$ and $s \simeq 10.7$ for $b = 1 \text{ } \mu\text{m}^2/\text{ms}$ (a), and $\kappa \simeq 7.4$ and $s \simeq 7.9$ for $b = 3 \text{ } \mu\text{m}^2/\text{ms}$ (b).

To examine if GFO also affords better sampling for purposes beyond powder averaging, we consider the performance across rotation schemes for higher order signal rotational invariants S_l , see Appendix.

When estimating a ground truth, we integrate using an Euler grid with exact quadrature on $\text{SO}(3)$ up to $L = 14$ (12,615 points), obtained as a direct product of a Gauss-Legendre grid (β) and 1D Fourier grids (α and γ). All simulations are performed in Matlab, and the code is open source at <https://github.com/Neurophysics-CFIN/GFO>.

VIII. RESULTS

To select optimal hyper parameters (V_{ll}) for GFO, we plot the band amplitude $\sqrt{E^l(S)}$ for $l = 0 - 14$ and signals generated from random diffusion tensors and $\mathbb{B} = \text{diag}(0, 1/3, 2/3)$ in Figs. 2. As expected, the signal energy is dominant at even l , and energy at $l = 1$ is exactly 0. Thus, for simplicity, our filter design neglects contributions from odd l . The amplitude decays rapidly with l , but the mean is well described by the Sobolev form $(1 + (l(l + 1))/\kappa^2)^{-s}$ with κ and s depending on b such that higher b -values increase the power at higher l .

Figure 3 shows the effect of GFO hyper parameters s and κ on the coefficient of variation

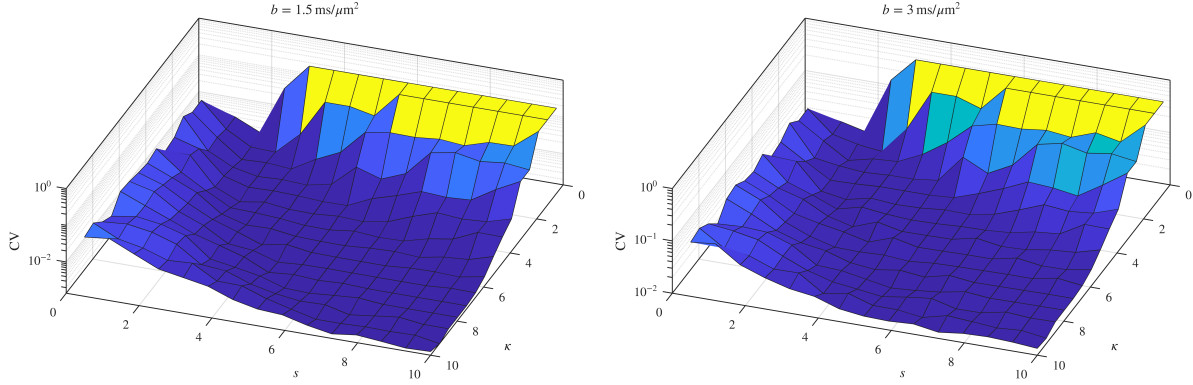


FIG. 3: The impact of hyper parameters s and κ in the GFO+ D_2 optimization is visualized in terms of the coefficient of variation (CV) of the signal powder average over 2601 $L = 6$ Euler grid rotations of the diffusion tensor. The underlying GFO set consisted of 24 rotations and was designed with $L = 8$. Two different b -values ($b = 1.5 \text{ } \mu\text{m}^2/\text{ms}$ left and $b = 3 \text{ } \mu\text{m}^2/\text{ms}$ right) are shown.

(CV) of powder average for an example diffusion and b -tensor at two b -values. Outside the low κ or low s regions, the CV is relatively flat, and this observation was consistent for other choices of B and D (not shown). The main effect of increasing b is to increase the overall CV. We will henceforth use $\kappa = 7$ and $s = 8$, comfortably in the flat region of the plots.

The performance of the rotation sets can be illustrated by their band powers $E_l(f)$, shown in Fig. 4. An ideal filter would have $E_l(f) = \delta_{l0}$ (Fig. 3, top left plot). All sets have $E_0(f) = 1$, but nonzero $E_l(f)$ for $l > 0$. This "spectral leakage" is generally highest for low N , and increases for increasing l as expected. The GFO has the smallest leakage for $l = 2$ and $l = 4$, where most signal power is concentrated (cf. Fig. 2). Both elstat and GFO improve markedly when accounting for the dihedral symmetry of the signal. Next, in Fig. 5, we present the CV for a single diffusion tensor $D = \text{diag}(0.1, 0.1, 2.8)$ probed with $\mathbb{B} = \text{diag}(0, 1/3, 2/3)$ in reciprocal units, as a function of the number of directions for all considered rotation schemes. The GFO scheme with D_2 symmetry exhibited the best performance with the lowest CV by a large margin. The full GFO had the second best performance, closely followed by the electrostatic repulsion with D_2 symmetry. The CV from the electrostatic scheme was still a bit higher, but better than quasi-uniform, and naive as well as random schemes had the worst performance. The benefit of GFO is exemplified in the lower left of Fig. 5, where it is seen to achieve a markedly narrower distribution of signal

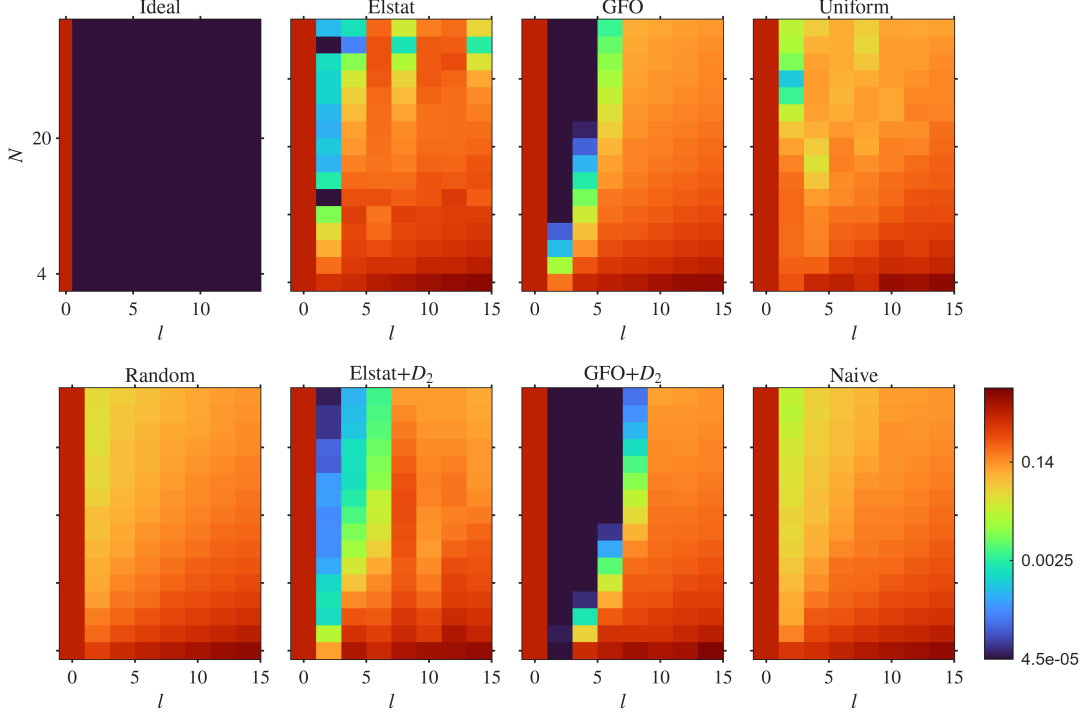


FIG. 4: The spectral profiles of the GFO filters show the best approximations to the ideal. The filter band powers $E_l(f)$ across l for different N and all schemes. The ideal filter has $E_l(f) = \delta_{l0}$ and is shown left most. Note the logarithmic color scale.

powder averages compared to electrostatic repulsion. The accuracy of all schemes, shown on the lower right, is very high, but overall worst for naive and uniform sets.

We also investigated whether GFO benefits other estimations that require rotated sampling. We estimated the first higher-order rotational invariant $S_2^2(b)$ as a function of b for all schemes with various N (Fig. 6). Throughout, GFO ($+D_2$) had superior precision compared to corresponding variants of electrostatic repulsion. Notably, biases were always positive owing to being squares of unbiased estimates $S_{mn}^l(b)$, and generally become worse when accounting for dihedral symmetry. A similar effect holds for LTE higher order invariants S_l , $l > 0$, partially explaining the poorer fits based on such features[29], as in RotInv[16]. As expected, accuracy generally improves with larger N , but the best method depends on N . Below $N \approx 48$, GFO is the more accurate, whereas at larger N , electrostatic repulsion is more accurate, at least at higher b values. This illustrates that optimizing for isotropy in $l = 0$ features does not automatically optimize for $l = 2$ features and above.

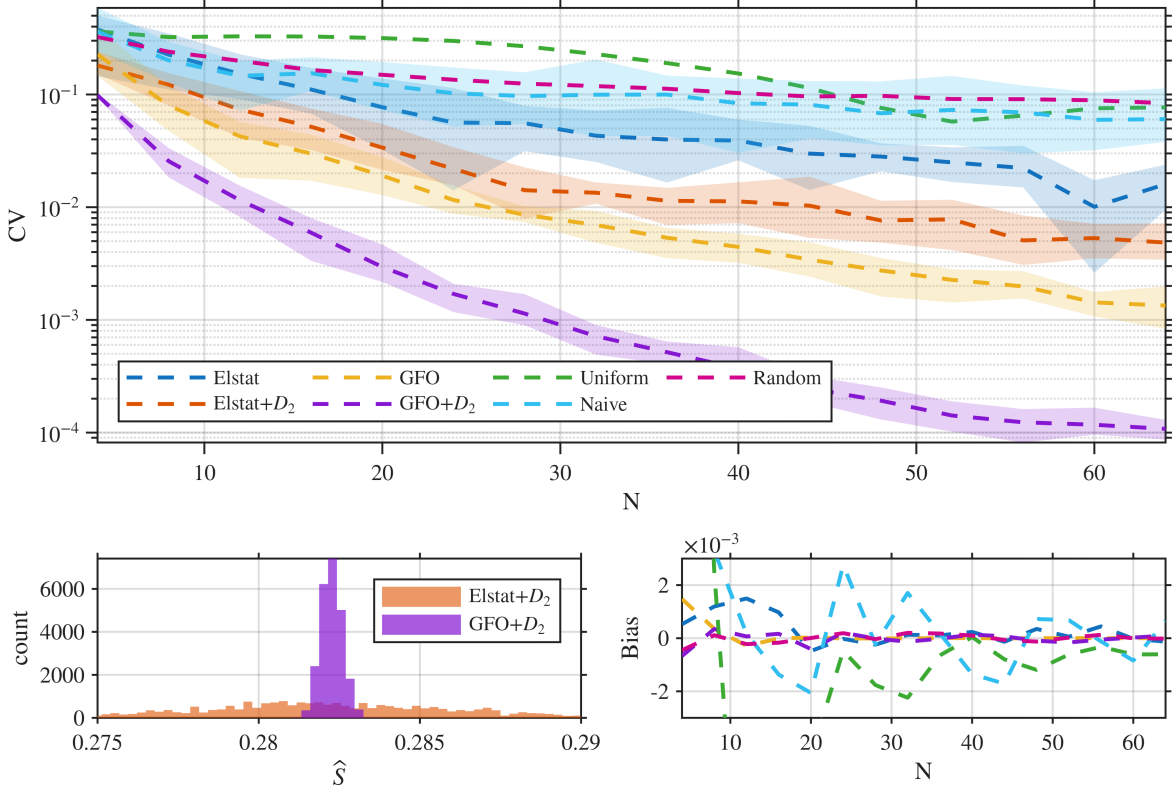


FIG. 5: The top plot shows that GFO has the best performance across the seven methods in terms of the coefficient of variation (CV) in the signal powder average (lower is better). Bottom left plot shows a representative histogram of powder averages at $N = 28$ wherein GFO produces a tighter distribution compared to electrostatic repulsion. The bottom right plot shows that all methods have negligible signal bias, but electrostatic repulsion and uniform sampling have the worst overall accuracy.

IX. DISCUSSION AND CONCLUSIONS

This work addresses a largely overlooked problem in diffusion MRI: how to design rotation sets that yield accurate powder averages when the diffusion encoding does not have a single symmetry axis? While it is well established that directions for linear b-tensor encoding can be optimized to be equidistant on the surface of a sphere[14, 21], the general case of triaxial b-tensor shapes requires uniform sampling over the rotation group $\text{SO}(3)$, for which fewer practical solutions exist[8, 23, 24, 30]. Indeed, we have shown that a naive application of existing rotation schemes to triaxial encoding is ill-advised as it can lead to substantial bias and variability in powder-averaged signals. We argue that this issue becomes increasingly

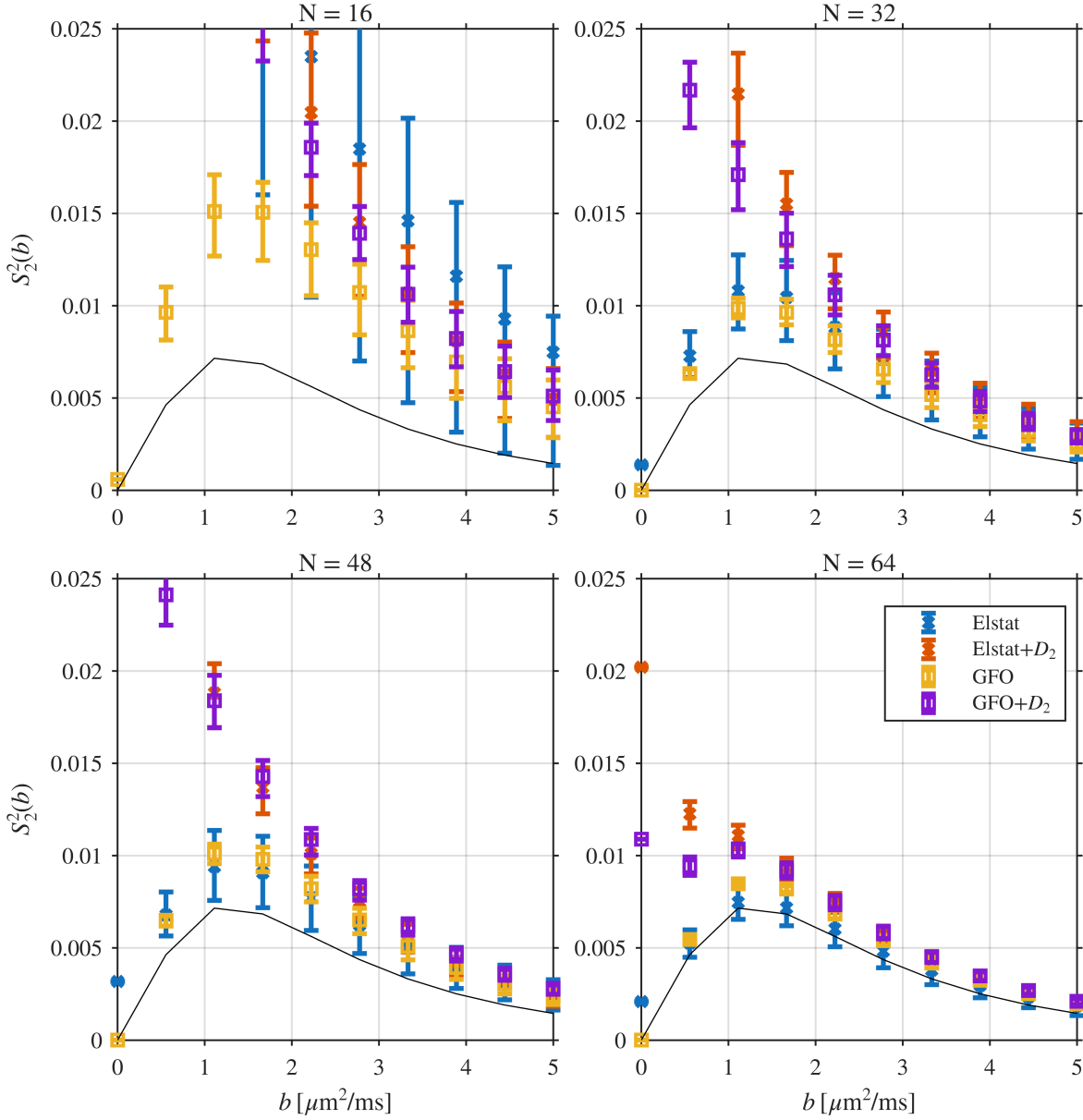


FIG. 6: The precision and accuracy of higher order rotational invariants also benefit from optimized sets. The figure compares S_2^2 for 16, 32, 48 and 64 directions for GFO and electrostatic repulsion variants. Ground truth is shown as solid black line, underlying signal generated with $\mathbb{B} = \text{diag}(0, 1/3, 2/3)$ and $\mathbb{D} = \text{diag}(0.1, 0.1, 2.8)$ in reciprocal units.

relevant as non-conventional encoding strategies are adopted.

Our solution to this problem, geometric filter optimization (GFO), provides a principled and effective solution that enables a categorical improvement in accuracy and precision without increasing scan time or placing additional demands on gradient system performance.

The central idea of GFO is to view a finite set of rotations as a sampling filter on $\text{SO}(3)$ and to optimize this filter to approximate the uniform distribution. Conceptually, the method aims to reduce the spectral leakage of the sampling filter into low-order $\text{SO}(3)$ harmonics that dominate the orientation-induced variance of powder averages.

GFO rotation sets consistently outperformed random, quasi-uniform, and electrostatic schemes by achieving substantially lower coefficient of variation and negligible bias. These improvements have several direct implications. First, GFO enables more efficient powder averaging, allowing a reduction in the number of rotations for a given performance level. Second, it naturally supports triaxial b-tensor encoding where no symmetry axis exists to simplify orientation sampling. Thus, the method is well suited for techniques that rely on triaxial encoding objects, such as skewness tensor imaging[31]. This benefit also extends to encoding features beyond the b-tensor, such as the orientation-dependent diffusion time effects in restriction-weighted q-space trajectory imaging[32]. Third, despite GFO being optimized for powder averaging ($l = 0$), for higher-order rotational invariants we observed a global improvement in precision and an improved accuracy at small to moderate N . This is relevant to rotation invariant analyses and model-based approaches that rely on these quantities. Finally, we expect that GFO rotation will benefit advanced microstructural models and protocols that combine multiple b-tensor shapes, including the Standard Model[33] and its exchange extensions, SMEX/NEXI[34, 35], as well as for correlation tensor imaging (CTI)[36, 37] which employs triaxial b-tensors.

In a preliminary analysis[38], we also examined whether post-hoc measurement weighting, as proposed by Knutsson et al.[25–27], could further improve powder averaging when applied to GFO and electrostatic rotation sets. While such weighting is known to substantially improve powder averaging for linear b-tensor encoding, we observed no meaningful improvement for GFO or other reasonably uniform $\text{SO}(3)$ sampling schemes. This likely reflects that GFO already provides near-uniform coverage of the relevant low-order $\text{SO}(3)$ harmonics, leaving little residual structure for post-hoc weighting to correct. For well-designed rotation sets, uniform weights therefore appear sufficient, simplifying both acquisition and analysis.

Several limitations should be noted. First, although GFO reduces bias in higher-order rotational invariants at low N , the bias can increase for larger N and higher b -values (see Fig. 6), and such performance may degrade further for $l > 2$ compared with schemes not

explicitly optimized for $l = 0$ as GFO. Second, all simulations were performed using noise-free signals assuming Gaussian diffusion. This isolates orientation-induced effects, but future work should assess robustness under realistic noise and more elaborate signal models. Third, only a limited set of b-tensor shapes was explored, and further work is warranted to map performance across the full space of possible encoding settings. Fourth, GFO relies on a Sobolev-type prior for the signal’s angular power spectrum; improved rotation sets may be achievable if better prior information about the signal is available.

Finally, while the use of GFO incurs no cost at scan time, generating the rotation sets requires a one-time offline optimization. On a good desktop computer, this takes on the order of 30 seconds for $N = 64$, which is negligible in practice and amortized over repeated use. An interesting extension of the present framework is the possibility of reversing the procedure to compute optimal weights for existing rotation sets, analogous to Knutsson weighting for LTE, which could retrospectively improve powder averages in previously acquired data.

In conclusion, GFO provides a general, efficient, and practically applicable framework for optimizing rotation sets in multidimensional diffusion MRI, enabling a categorical improvement in accuracy and precision of the powder-averaged signal in measurements that include triaxial diffusion encoding.

ACKNOWLEDGMENTS

The authors thank Noam Shemesh and Dmitry Novikov for discussions. This work was partially supported by Lundbeck Foundation grant 10.46540/3103-00144B, the Swedish Cancer Society grant 22 0592 JIA, and the Crafoord Foundation grant 20240791. SNJ is also grateful for support from The Danish Research Foundation. Generative AI tools, specifically ChatGPT, were utilized in this research to assist in code and text drafting. The AI outputs have been rigorously verified for accuracy, and their use has been disclosed in compliance with the University’s guidelines. The researchers take full responsibility for all outputs.

Financial disclosure

None reported.

Conflict of interest

The authors declare no potential conflict of interests.

X. APPENDIX

To exemplify and motivate the consideration of higher order rotational invariants in the context of $\text{SO}(3)$, we here consider generalizations of the Standard Model of diffusion in white matter to triaxial diffusion and B-tensors. It will be convenient to define \mathbb{B} and \mathbb{D} as the B and diffusion tensors in their respective principal frames, given by rotations h and g of the lab system. The Standard Model of diffusion in white matter[33] can be formulated in terms of an $\text{SO}(3)$ convolution with $f_1(h) = \mathcal{P}(h\hat{e}_3)$, the fiber ODF, and $f_2(h) = \mathcal{K}(\text{Tr}(h\mathbb{B}h^{-1}\mathbb{D}))$ the kernel:

$$\begin{aligned} S(\mathbb{B}) &= \int_{\text{S}^2} \mathcal{P}(\hat{n}) \mathcal{K}(\text{Tr}(\mathbb{B}\mathbb{D})) d\hat{n} \\ &= \int_{\text{SO}(3)} \mathcal{P}(g\hat{e}_3) \mathcal{K}(\text{Tr}(h\mathbb{B}h^{-1}g\mathbb{D}g^{-1})) dg \\ &= \int_{\text{SO}(3)} \mathcal{P}(g\hat{e}_3) \mathcal{K}(\text{Tr}(g^{-1}h\mathbb{B}h^{-1}g\mathbb{D})) dg \\ &= \int_{\text{SO}(3)} \mathcal{P}(hg^{-1}\hat{e}_3) \mathcal{K}(\text{Tr}(g\mathbb{B}g^{-1}\mathbb{D})) dg. \end{aligned}$$

We consider generalizations of the standard model by allowing triaxial diffusion tensors and encoding tensors – that is, matrices with 3 distinct eigenvalues. In the former case, the fiber orientation distribution function, fODF, instead becomes a distribution of frames (eigen systems for the local fascicle) $\mathcal{P}(h)$, and the signal for a given b-tensor rotation, $\mathbb{B} = h\mathbb{B}h^{-1}$, becomes

$$S(h) = \int_{\text{SO}(3)} \mathcal{P}(hg^{-1}) \mathcal{K}(g) dg \iff S^l = \mathcal{P}^l \mathcal{K}^l.$$

As mentioned in the main text, the dihedral (D_2) symmetry of the signal leads to selection rules for n even and $l \neq 1$.

Furthermore, for axially symmetric \mathbb{B} , $\mathcal{K}_{mn}^l \propto \delta_{n0}$, whereas uniaxial \mathbb{D} leads to $\mathcal{K}_{mn}^l \propto \delta_{m0}$. Combined, this leads to the standard factorization of the Standard Model[33]. Incidentally, this means that for data acquired with linear b-tensor encoding, the matrix $S_{m0}^l(b)$ for fixed l with m along rows and b along columns,

$$S_{m0}^l(b) = \mathcal{P}_{mk}^l \mathcal{K}_{k0}^l(b),$$

has rank > 1 if the microscopic tensors \mathbb{D} are not uniaxial – thereby suggesting a test for the detection of triaxial diffusion tensors. Thus, the findings in Ref. [39] indicate that triaxial tensors are at least hard to observe on standard clinical scans. As for linear b-tensor encoding[16], we can define rotation invariant signal scalars as

$$S_l^2 \equiv \frac{1}{2l+1} \sum_{mn} |S_{mn}^l|^2,$$

where $0 \leq S_l \leq 1$. The S_l can be used as new contrasts or for fitting analogously to the RotInv framework[16].

[1] E. O. Stejskal and J. E. Tanner, Spin Diffusion Measurements: Spin Echoes in the Presence of a Time-Dependent Field Gradient, *J Chem Phys* **42**, 288 (1965).

[2] Y. Cheng and D. G. Cory, Multiple scattering by NMR, *J. Am. Chem. Soc.* **121**, 7935 (1999).

[3] N. Shemesh, S. N. Jespersen, D. C. Alexander, Y. Cohen, I. Drobnjak, T. B. Dyrby, J. Finsterbusch, M. A. Koch, T. Kuder, F. Laun, M. Lawrenz, H. Lundell, P. P. Mitra, M. Nilsson, E. Ozarslan, D. Topgaard, and C. F. Westin, Conventions and nomenclature for double diffusion encoding NMR and MRI, *Magn Reson Med* **75**, 82 (2016).

[4] F. Szczepankiewicz, C. F. Westin, and M. Nilsson, Gradient waveform design for tensor-valued encoding in diffusion MRI, *J Neurosci Methods* **348**, 109007 (2021).

[5] D. Topgaard, Multidimensional diffusion MRI, *J Magn Reson* **275**, 98 (2017).

[6] C. F. Westin, H. Knutsson, O. Pasternak, F. Szczepankiewicz, E. Ozarslan, D. van Westen, C. Mattisson, M. Bogren, L. J. O'Donnell, M. Kubicki, D. Topgaard, and M. Nilsson, Q-space trajectory imaging for multidimensional diffusion MRI of the human brain, *NeuroImage* **135**, 345 (2016).

[7] S. Lasić, F. Szczepankiewicz, S. Eriksson, M. Nilsson, and D. Topgaard, Microanisotropy imaging: Quantification of microscopic diffusion anisotropy and orientational order parameter by diffusion MRI with magic-angle spinning of the q-vector, *Frontiers in Physics* **2**, 10.3389/fphy.2014.00011 (2014).

[8] S. N. Jespersen, H. Lundell, C. K. Sønderby, and T. B. Dyrby, Orientationally invariant metrics of apparent compartment eccentricity from double pulsed field gradient diffusion experiments, *NMR in Biomedicine* **26**, 1647 (2013).

[9] F. Szczepankiewicz, D. van Westen, E. Englund, C. F. Westin, F. Stahlberg, J. Latt, P. C. Sundgren, and M. Nilsson, The link between diffusion MRI and tumor heterogeneity: Mapping cell eccentricity and density by diffusional variance decomposition (DIVIDE), *NeuroImage* **142**, 522 (2016).

[10] S. Coelho, J. M. Pozo, S. N. Jespersen, D. K. Jones, and A. F. Frangi, Resolving degeneracy in diffusion MRI biophysical model parameter estimation using double diffusion encoding, *Magn Reson Med* **82**, 395 (2019).

[11] M. Reisert, V. G. Kiselev, and B. Dhital, A unique analytical solution of the white matter standard model using linear and planar encodings, *Magn Reson Med* 10.1002/mrm.27685 (2019).

[12] S. Coelho, S. H. Baete, G. Lemberskiy, B. Ades-Aron, G. Barrol, J. Veraart, D. S. Novikov, and E. Fieremans, Reproducibility of the Standard Model of diffusion in white matter on clinical MRI systems, *NeuroImage* **257**, 119290 (2022).

[13] B. Lampinen, F. Szczepankiewicz, J. Latt, L. Knutsson, J. Martensson, I. M. Bjorkman-Burtscher, D. van Westen, P. C. Sundgren, F. Stahlberg, and M. Nilsson, Probing brain tissue microstructure with MRI: Principles, challenges, and the role of multidimensional diffusion-relaxation encoding, *NeuroImage* **282**, 120338 (2023).

[14] M. Bak and N. C. Nielsen, REPULSION, A Novel Approach to Efficient Powder Averaging in Solid-State NMR, *Journal of Magnetic Resonance* **125**, 132 (1997).

[15] E. Kaden, F. Kruggel, and D. C. Alexander, Quantitative mapping of the per-axon diffusion coefficients in brain white matter, *Magn Reson Med* **75**, 1752 (2016).

[16] D. S. Novikov, J. Veraart, I. O. Jelescu, and E. Fieremans, Rotationally-invariant mapping of scalar and orientational metrics of neuronal microstructure with diffusion MRI, *NeuroImage* **174**, 518 (2018).

[17] F. Szczepankiewicz, J. Sjölund, F. Ståhlberg, J. Lätt, and M. Nilsson, Tensor-valued diffusion encoding for diffusional variance decomposition (DIVIDE): Technical feasibility in clinical MRI systems, *PLOS ONE* **14**, e0214238 (2019).

[18] M. Edén, Computer simulations in solid-state NMR. III. Powder averaging, *Concepts in Magnetic Resonance Part A* **18A**, 24 (2003).

[19] E. T. McKinnon, J. H. Jensen, G. R. Glenn, and J. A. Helpern, Dependence on b-value of the direction-averaged diffusion-weighted imaging signal in brain, *Magnetic Resonance Imaging*

36, 121 (2017).

[20] J. Veraart, D. Nunes, U. Rudrapatna, E. Fieremans, D. K. Jones, D. S. Novikov, and N. Shemesh, Noninvasive quantification of axon radii using diffusion MRI, *Elife* **9**, 10.7554/eLife.49855 (2020).

[21] D. Jones, M. Horsfield, and A. Simmons, Optimal strategies for measuring diffusion in anisotropic systems by magnetic resonance imaging, *Magnetic Resonance in Medicine* **42**, 515 (1999).

[22] M. Gräf and D. Potts, Sampling Sets and Quadrature Formulae on the Rotation Group, *Numer Func Anal Opt* **30**, 665 (2009).

[23] S. N. Jespersen, Isotropic sampling of tensor-encoded diffusion MRI, *Magnetic Resonance in Medicine* **93**, 2040 (2025).

[24] C.-F. Westin and F. Szczepankiewicz, Isotropic sampling for skewed encoding: novel rotation schemes for non-axisymmetric encoding objects in diffusion mri, *Proceedings of the International Society for Magnetic Resonance in Medicine* **28** (2020).

[25] H. Knutsson, M. Andersson, and J. Wiklund, Advanced filter design, *Proceedings of the 11th Scandinavian Conference on Image Analysis* (1999).

[26] M. Afzali, H. Knutsson, E. Özarslan, and D. K. Jones, Computing the orientational-average of diffusion-weighted MRI signals: A comparison of different techniques, *Scientific Reports* **11**, 14345 (2021).

[27] F. Szczepankiewicz, C.-F. Westin, and H. Knutsson, A measurement weighting scheme for optimal powder average estimation, *Proceedings of the International Society for Magnetic Resonance in Medicine* **25** (2017).

[28] A. Yershova, S. Jain, S. M. LaValle, and J. C. Mitchell, Generating Uniform Incremental Grids on $SO(3)$ Using the Hopf Fibration, *The International Journal of Robotics Research* **29**, 801 (2010).

[29] G. París, T. Pieciak, D. K. Jones, S. Aja-Fernández, A. Tristán-Vega, and J. Veraart, Thermal noise lowers the accuracy of rotationally invariant harmonics of diffusion MRI data and their robustness to experimental variations, *Magnetic Resonance in Medicine* **95**, 204 (2026).

[30] H. Lundell, T. B. Dyrby, P. L. Hubbard, F.-L. Zhou, G. J. Parker, and S. N. Jespersen, Validation of double diffusion schemes of microscopic fractional anisotropy, *Proc. Int. Soc. Magn. Reson. Med.*, *Proceedings of the International Society for Magnetic Resonance in Medicine*

23 (2016).

- [31] L. Ning, F. Szczepankiewicz, M. Nilsson, Y. Rathi, and C.-F. Westin, Probing tissue microstructure by diffusion skewness tensor imaging, *Scientific Reports* **11**, 135 (2021).
- [32] F. Szczepankiewicz, M. Molendowska, S. Lasić, M. E. Safi, M. Gottschalk, E. Sereti, A. Bjartell, L. Knutsson, O. V. Timmermand, C. Ceberg, and J. Strand, Restriction-weighted q-space trajectory imaging (ResQ): Toward mapping diffusion time effects with tensor-valued diffusion encoding in human prostate cancer xenografts, *bioRxiv* , 2025.12.08.692924 (2025).
- [33] D. S. Novikov, E. Fieremans, S. N. Jespersen, and V. G. Kiselev, Quantifying brain microstructure with diffusion MRI: Theory and parameter estimation, *NMR Biomed* **32**, e3998 (2019).
- [34] J. L. Olesen, L. Østergaard, N. Shemesh, and S. N. Jespersen, Diffusion time dependence, power-law scaling, and exchange in gray matter, *NeuroImage* **251**, 118976 (2022).
- [35] I. O. Jelescu, A. de Skowronski, F. Geffroy, M. Palombo, and D. S. Novikov, Neurite Exchange Imaging (NEXI): A minimal model of diffusion in gray matter with inter-compartment water exchange, *NeuroImage* **256**, 119277 (2022).
- [36] R. N. Henriques, S. N. Jespersen, and N. Shemesh, Correlation tensor magnetic resonance imaging, *NeuroImage* **211**, 116605 (2020).
- [37] R. N. Henriques, M. Palombo, S. N. Jespersen, N. Shemesh, H. Lundell, and A. Ianus, Double diffusion encoding and applications for biomedical imaging, *J Neurosci Methods* **348**, 108989 (2021).
- [38] S. N. Jespersen and F. Szczepankiewicz, Accurate powder averaging in dmri by optimal encoding rotations and signal weighting, *Proceedings of the International Society for Magnetic Resonance in Medicine* **34** (2026).
- [39] D. Christiaens, J. Veraart, L. Cordero-Grande, A. N. Price, J. Hutter, J. V. Hajnal, and J. D. Tournier, On the need for bundle-specific microstructure kernels in diffusion MRI, *NeuroImage* **208**, 116460 (2020).